Inorganic Chemistry
Article

Inorg. Chem. **2010**, *49*, 823–832 **823**
DOI: 10.1021/ic900586e

New Series of Ruthenium(II) and Osmium(II) Complexes Showing Solid-State Phosphorescence in Far-Visible and Near-Infrared

Jing-Lin Chen,[†] Yun Chi,* and Kellen Chen

Department of Chemistry, National Tsing Hua University, Hsinchu 30013, Taiwan. [†]Present address: School of Material and Chemical Engineering, Jiangxi University of Science and Technology, Ganzhou, Jiangxi 341000, China.

Yi-Ming Cheng, Min-Wen Chung, Ya-Chien Yu, Gene-Hsiang Lee, and Pi-Tai Chou*

Department of Chemistry and Instrumentation Center, National Taiwan University, Taipei 106, Taiwan

Ching-Fong Shu

Department of Applied Chemistry, National Chiao Tung University, Hsinchu 30010, Taiwan

Received March 26, 2009

A new Ru^{II} complex, $[Ru(fpbpymH)_2]Cl_2$ (**1**), in which fpbpymH = [5-(trifluoromethyl)pyrazol-3-yl](2,2′-bipyrid-6-yl)methane, was prepared by the treatment of $[Ru(DMSO)_4Cl_2]$ with 2 equiv of the terdentate chelate fpbpymH in refluxing ethanol. A single-crystal X-ray diffraction study of **1** revealed a distorted octahedral Ru^{II} framework, showing strong N−H···Cl hydrogen bonding between the fpbpymH ligand and Cl anions. In the presence of Na_2CO_3, the methylene linkers of chelates in **1** underwent stepwise oxygenation, forming the charge-neutral complexes [Ru(fpbpym)(fpbpyk)] (**2**) and $[Ru(fpbpyk)_2]$ (**3**) [fpbpykH = [5-(trifluoromethyl)pyrazol-3-yl](2,2′-bipyrid-6-yl) ketone] in sequence. The respective charge-neutral Os^{II} complex $[Os(fpbpyk)_2]$ (**4**) was also isolated by the treatment of $OsCl_3 \cdot 3H_2O$ with 2 equiv of the terdentate chelate fpbpymH. Electrochemical analysis indicated that the introduction of the electron-withdrawing ketone group in **2**−**4** increased the metal-based oxidation potential in sequence. For the photophysical properties, complexes **1**−**4** are essentially nonluminescent in solution (e.g., CH_2Cl_2 or MeOH) at room temperature, but all exhibit 600−1100 nm phosphorescence with moderate intensity for the powdery, solid sample at room temperature. The trend in terms of the emission peak wavelength of **1** (666 nm) < **3** (795 nm) < **2** (810 nm) < **4** (994 nm) among titled complexes is in agreement with the corresponding onset of absorption spectra as well as the time-dependent density functional theory calculation of **1** < **3** < **2** < **4**.

1. Introduction

Since the first preparation of the 2,2′:6′,2″-terpyridine (tpy) chelate was reported over 75 years ago,[1] the chemistry of tpy-based, transition-metal complexes has been the target of extensive investigation.[2] In particular, the respective Ru^{II} and Os^{II} complexes have exhibited excellent chemical stability, reversible redox processes, and good absorptivity and luminescence in visible and near-infrared (NIR) regions.[3] Recently, the fast development of transition-metal-based supramolecular chemistry has also revitalized relevant research on bis-terdentate Ru^{II} and Os^{II} complexes. This is mainly attributed to the fact that, upon insertion of conjugated π bridges between these complexes, the resulting rodlike donor−sensitizer−acceptor molecular assemblies are capable of executing directional electron and/or energy transfers with high efficiencies.[4]

*To whom correspondence should be addressed. E-mail: ychi@mx.nthu.edu.tw (Y.C.), chop@ntu.edu.tw (P.-T.C.). Fax: +886 3 572 0864 (Y.C.), +886 2 2369 5208 (P.-T.C.).

(1) Morgan, G. T.; Burstall, F. H. *J. Chem. Soc.* **1932**, 20.

(2) (a) Constable, E. C. *Prog. Inorg. Chem.* **1994**, *42*, 67. (b) Cargill Thompson, A. M. W. *Coord. Chem. Rev.* **1997**, *160*, 1.

(3) (a) Campagna, S.; Puntoriero, F.; Nastasi, F.; Bergamini, G.; Balzani, V. *Top. Curr. Chem.* **2007**, *280*, 117. (b) Kumaresan, D.; Shankar, K.; Vaidya, S.; Schmehl, R. H. *Top. Curr. Chem.* **2007**, *281*, 101.

(4) (a) Sauvage, J. P.; Collin, J.-P.; Chambron, J.-C.; Guillerez, S.; Coudret, C.; Balzani, V.; Barigelletti, F.; De Cola, L.; Flamigni, L. *Chem. Rev.* **1994**, *94*, 993. (b) Zeng, F.; Zimmerman, S. C. *Chem. Rev.* **1997**, *97*, 1681. (c) Flamigni, L.; Barigelletti, F.; Armaroli, N.; Collin, J.-P.; Dixon, I. M.; Sauvage, J.-P.; Williams, J. A. G. *Coord. Chem. Rev.* **1999**, *190*, 671. (d) Collin, J.-P.; Dietrich-Buchecker, C.; Gavina, P.; Jimenez-Molero, M. C.; Sauvage, J.-P. *Acc. Chem. Res.* **2001**, *34*, 477.

Published on Web 12/23/2009

Chart 1

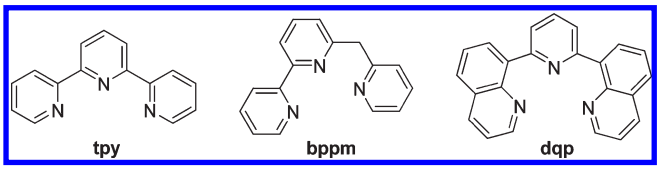

Accordingly, much effort has been made in the design and synthesis of terdentate polypyridine ligands to improve the photophysical properties of the corresponding Ru^{II} and Os^{II} complexes.[5] The typical approach takes advantage of the substituent effects for tuning the energy gap of ^{3}MLCT and ^{3}MC states,[6] which involves the insertion of judiciously selected heterocyclic substituents to the tpy chelate.[7] Also, an increase of the ligand bite angle[8] was attempted by making the complex adopt a less distorted octahedral arrangement and hence increased the ligand field strength and reduced the nonradiative decay. For instance, as shown in Chart 1, when one methylene group is introduced between the pyridyl units of terpyridine, the ligand bite angle of the corresponding complex $[Ru(bppm)_2]^{2+}$ (bppm = [6-(2,2′-bipyridyl)(2-pyridyl)methane]) is increased, affording a longer excited-state lifetime (17−18 ns) relative to its parent complex $[Ru(tpy)_2]^{2+}$ (0.25 ns),[9] for which the shortened lifetime is most probably due to the distortion of metal−ligand bonding away from the perfect octahedral arrangement. This leads to a decrease of the ligand field strength and a stabilization of the nonemissive d−d excited states relative to the desired metal-to-ligand charge-transfer (MLCT) excited state.[4a] Furthermore, employing 2,6-bis(quinolin-8-yl)pyridine (bqp), because of its capability of forming double hexagonal metallacycles, could, in turn, reduce the strain energy. As a consequence, the as-prepared octahedral complex $[Ru(bqp)_2]^{2+}$ shows a markedly enhanced excited-state lifetime of 3.0 μs at room temperature.[10] It is thus feasible that the enlargement of the ligand bite angle may gain positive impact on the improvement of both the chemical stabilities and photophysical properties of metal complexes.

Chart 2

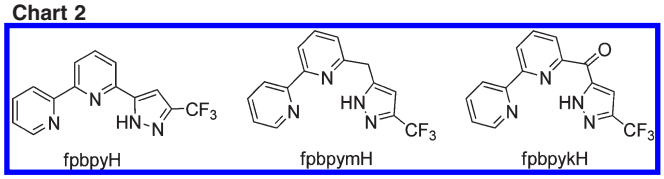

Chart 3

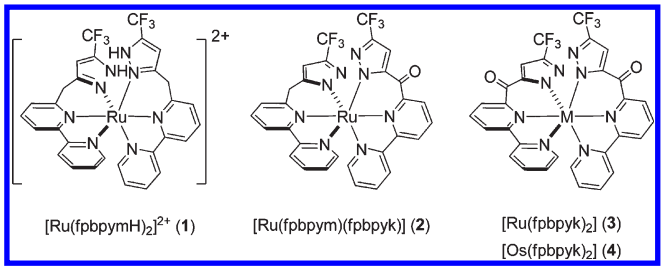

Alternatively, being ascribed to a class of terdentate chelate 6-(5-trifluoromethyl-pyrazol-3-yl)-2,2′-bipyridine (fpbpyH; Chart 2) has latent potential for the preparation of various luminescent metal complexes for organic light emitting diodes (OLEDs)[11] as well as dye-sensitized solar cell (DSSC) applications.[12] Particularly, the related bidentate azolate chelates have been widely utilized in obtaining emissive Ru^{II}, Os^{II}, Ir^{III}, and Pt^{II} metal complexes that are useful for the fabrication of highly efficient phosphorescent OLEDs.[13,14] Encouraged by these successful attempts, we decided to shift our research endeavors to the [5-(trifluoromethyl)pyrazol-3-yl](2,2′-bipyrid-6-yl)methane (fpbpymH) ligand, which is a modification of the respective terdentate fpbpyH. Upon introduction of a saturated methylene linker, fpbpymH would exhibit better skeletal flexibility in a manner similar to that of the bppm and bqp chelates discussed earlier. It is thus of great interest to know if such a modification has any effect on the chemical and photophysical properties versus those synthesized using its parent fpbpyH chelate as well as the oxidized fbppykH analogue, [5-(trifluoromethyl)-pyrazol-3-yl](2,2′-bipyrid-6-yl) ketone (see Chart 2).

Herein, we describe the syntheses and structural and photophysical studies of three Ru^{II} complexes **1**−**3** emanating from the reaction of the terdentate fpbpymH with a $[Ru(DMSO)_4Cl_2]$ reagent, among which **2** and **3** are obtained from a ligand oxidation occurring on their predecessor **1** (see Chart 3). On the other hand, the reaction of fpbpymH with $OsCl_3$ failed to afford nonoxidized and partially oxidized

(5) (a) Hammarström, L.; Barigelletti, F.; Flamigni, L.; Indelli, M. T.; Armaroli, N.; Calogero, G.; Guardigli, M.; Sour, A.; Collin, J.-P.; Sauvage, J. P. *J. Phys. Chem. A* **1997**, *101*, 9061. (b) Medlycott, E. A.; Hanan, G. S. *Chem. Soc. Rev.* **2005**, *34*, 133. (c) Harriman, A.; Ziessel, R. *Chem. Commun.* **1996**, 1707. (d) Medlycott, E. A.; Hanan, G. S. *Coord. Chem. Rev.* **2006**, *250*, 1763.
(6) (a) Maestri, M.; Armaroli, N.; Balzani, V.; Constable, E. C.; Thompson, A. M. W. *Inorg. Chem.* **1995**, *34*, 2759. (b) Benniston, A. C.; Harriman, A.; Grosshenny, V.; Ziessel, R. *New J. Chem.* **1997**, *21*, 405. (c) Benniston, A. C.; Grosshenny, V.; Harriman, A.; Ziessel, R. *Angew. Chem., Int. Ed.* **1994**, *33*, 1884. (d) Fang, Y.-Q.; Taylor, N. J.; Hanan, G. S.; Loiseau, F.; Passalacqua, R.; Campagna, S.; Nierengarten, H.; van Dorsselaer, A. *J. Am. Chem. Soc.* **2002**, *124*, 7912.
(7) (a) Beley, M.; Chodorowski, S.; Collin, J.-P.; Sauvage, J.-P.; Flamigni, L.; Barigelletti, F. *Inorg. Chem.* **1994**, *33*, 2543. (b) Mano, A.; Stefio, I.; Poggi, A.; Tringali, C.; Di Pietro, C.; Campagna, S. *New J. Chem.* **1997**, *21*, 1173. (c) Duati, M.; Tasca, S.; Lynch, F. C.; Bohlen, H.; Vos, J. G.; Stagni, S.; Ward, M. D. *Inorg. Chem.* **2003**, *42*, 8377.
(8) (a) Abrahamsson, M.; Wolpher, H.; Johansson, O.; Larsson, J.; Kritikos, M.; Eriksson, L.; Norrby, P.-O.; Bergquist, J.; Sun, L.; Åkermark, B.; Hammarström, L. *Inorg. Chem.* **2005**, *44*, 3215. (b) Abrahamsson, M.; Becker, H.-C.; Hammarström, L.; Bonnefous, C.; Chamchoumis, C.; Thummel, R. P. *Inorg. Chem.* **2007**, *46*, 10354.
(9) Wolpher, H.; Johansson, O.; Abrahamsson, M.; Kritikos, M.; Sun, L.; Åkermark, B. *Inorg. Chem. Commun.* **2004**, *7*, 337.
(10) (a) Abrahamsson, M.; Jäger, M.; Österman, T.; Eriksson, L.; Persson, P.; Becker, H.-C.; Johansson, O.; Hammarström, L. *J. Am. Chem. Soc.* **2006**, *128*, 12616. (b) Abrahamsson, M.; Jaeger, M.; Kumar, R. J.; Oesterman, T.; Persson, P.; Becker, H.-C.; Johansson, O.; Hammarstroem, L. *J. Am. Chem. Soc.* **2008**, *130*, 15533.
(11) (a) Chi, Y.; Chou, P.-T. *Chem. Soc. Rev.* **2007**, *36*, 1421. (b) Chen, K.; Cheng, Y.-M.; Chi, Y.; Ho, M.-L.; Lai, C.-H.; Chou, P.-T.; Peng, S.-M.; Lee, G.-H. *Chem. Asian J.* **2007**, *2*, 155. (c) Song, Y.-H.; Chiu, Y.-C.; Chi, Y.; Chou, P.-T.; Cheng, Y.-M.; Lin, C.-W.; Lee, G.-H.; Carty, A. J. *Organometallics* **2008**, *27*, 80. (d) Chi, Y.; Chou, P.-T. *Chem. Soc. Rev.* **2010**, DOI: 10.1039/b916237b.
(12) (a) Chen, K.-S.; Liu, W.-H.; Wang, Y.-H.; Lai, C.-H.; Chou, P.-T.; Lee, G.-H.; Chen, K.; Chen, H.-Y.; Chi, Y.; Tung, F.-C. *Adv. Funct. Mater.* **2007**, *17*, 2964. (b) Chen, K.; Hong, Y.-H.; Chi, Y.; Liu, W.-H.; Chen, B.-S.; Chou, P.-T. *J. Mater. Chem.* **2009**, *19*, 5329. (c) Chen, B.-S.; Chen, K.; Hong, Y.-H.; Liu, W.-H.; Li, T.-H.; Lai, C.-H.; Chou, P.-T.; Chi, Y.; Lee, G.-H. *Chem. Commun.* **2009**, 5844.
(13) (a) Chou, P.-T.; Chi, Y. *Eur. J. Inorg. Chem.* **2006**, 3319. (b) Chou, P.-T.; Chi, Y. *Chem.—Eur. J.* **2007**, *13*, 380.
(14) (a) Yang, C.-H.; Cheng, Y.-M.; Chi, Y.; Hsu, C.-J.; Fang, F.-C.; Wong, K.-T.; Chou, P.-T.; Chang, C.-H.; Tsai, M.-H.; Wu, C.-C. *Angew. Chem., Int. Ed.* **2007**, *46*, 2418. (b) Niu, Y.-H.; Liu, M. S.; Ka, J.-W.; Bardeker, J.; Zin, M. T.; Schofield, S.; Chi, Y.; Jen, A. K.-Y. *Adv. Mater.* **2007**, *19*, 300. (c) Hwang, K.-C.; Chen, J.-L.; Chi, Y.; Lin, C.-W.; Cheng, Y.-M.; Lee, G.-H.; Chou, P.-T.; Lin, S.-Y.; Shu, C.-F. *Inorg. Chem.* **2008**, *47*, 3307.

derivatives, namely, $[Os(fpbpymH)_2]^{2+}$ and [Os(fpbpym)(fpbpyk)], but only the doubly oxidized product $[Os(fpbpyk)_2]$ (**4**). The successful isolation of **2**−**4** demonstrates a higher tendency to form the fpbpyk chelate, which could be due to the synergism involving the greater π stabilization induced by the carbonyl group and facile oxidation at the activated position in the ligand framework of Ru^{II}-based polypyridophenazine complexes.[15] Moreover, the methylene-to-carbonyl conversion discussed, which is similar to what occurred in 2,6-bis(2-pyridylmethyl)pyridine,[16] caused the resulting fpbpyk ligand to afford a much reduced ligand-centered energy gap, as evidenced by their photophysical and electrochemical data elaborated in the following sections.

2. Experimental Section

General Information and Materials. All reactions were performed under a nitrogen atmosphere using anhydrous solvents or solvents treated with an appropriate drying reagent. Oxygen-$^{18}O_2$, 97 atom % ^{18}O, was purchased from ISOTEC. Mass spectra were obtained on a JEOL SX-102A instrument operating in electron impact (EI) or fast atom bombardment (FAB) mode. ^1H and ^{19}F NMR spectra were recorded on a Varian Mercury-400 or INOVA-500 instrument. Elemental analyses were conducted at the NSC Regional Instrumentation Center at National Chiao Tung University.

The targeted fpbpymH chelate was prepared in three consecutive steps. First, 6-methyl-2,2′-bipyridine was obtained from the reaction of 2,2′-bipyridine with methyllithium and oxidative workup,[17] while 6-acetonyl-2,2′-bipyridine was obtained from lithiation of 6-methyl-2,2′-bipyridine with lithium diisopropylamide at −78 °C and subsequent treatment with dimethylacetamide.[18] Finally, the fpbpymH ligand was synthesized by condensation of 6-acetonyl-2,2′-bipyridine and ethyl trifluoroacetate, followed by cyclization with an excess of hydrazine hydrate in refluxing ethanol.[17,19]

Preparation of [5-(Trifluoromethyl)pyrazol-3-yl](2,2′-bipyrid-6-yl)methane (fpbpymH). To a stirred mixture of NaOEt (1.2 g, 17.63 mmol) and THF (45 mL) at 0 °C was added a 30 mL solution of 6-acetonyl-2,2′-bipyridine (2.5 g, 11.78 mmol) in THF, followed by the addition of ethyl trifluoroacetate (2.1 mL, 17.62 mmol). The mixture was allowed to heat for 12 h at 80 °C and then was quenched with 2 M HCl until pH 5−6. The resulting mixture was extracted with CH_2Cl_2 (3 × 80 mL). The combined extracts were washed with water, dried over anhydrous Na_2SO_4, and concentrated under vacuum to give the corresponding β-diketone compound (3.5 g).

Without further purification, hydrazine monohydrate (98%, 3.0 mL, 62 mmol) was added into a solution of the β-diketone reagent in EtOH (50 mL). After reflux for 12 h, the solvent was evaporated. The residue was dissolved in CH_2Cl_2 (100 mL), and the solution was washed with water, dried over anhydrous Na_2SO_4, and concentrated. Finally, the product was purified by silica gel column chromatography using a 7:3 mixture of CH_2Cl_2 and ethyl acetate, giving the terdentate ligand fpbpymH as a white solid. Yield: 1.3 g, 4.27 mmol, 36%.

Spectral data for fpbpymH: EI-MS m/z 304 (M^+); ^1H NMR (500 MHz, $CDCl_3$) δ 11.80 (s, 1H), 8.71 (d, J = 5.0 Hz, 1H), 8.25 (t, J = 9.0 Hz, 2H), 7.86 (td, J = 7.8 and 1.7 Hz, 1H), 7.79 (t, J = 8.0 Hz, 1H), 7.37−7.33 (m, 1H), 7.24 (d, J = 7.0 Hz, 1H), 6.43 (s, 1H), 4.26 (s, 2H); ^{19}F NMR (470 MHz, $CDCl_3$) δ −62.13 (s, 3F).

Preparation of $[Ru(fpbpymH)_2]Cl_2$ (1). A mixture of $Ru(DMSO)_4Cl_2$ (97 mg, 0.200 mmol) and fpbpymH (129 mg, 0.424 mmol) in ethanol (30 mL) was refluxed for 12 h under a nitrogen atmosphere. After the mixture was cooled to room temperature, the solvent was removed under vacuum. The residue was recrystallized from a saturated CH_2Cl_2 and ethanol mixture (15:1) to give dark-brown crystals. Yield: 80 mg, 0.102 mmol, 51%. Single crystals were obtained upon placement of the supersaturated solution of **1** in a 1:20 mixture of methanol and CH_2Cl_2.

Spectral data for 1: ^1H NMR (500 MHz, methanol-d_4, 298 K) δ 8.65 (d, J = 8.5 Hz, 2H), 8.43 (d, J = 7.5 Hz, 2H), 8.33 (t, J = 8.0 Hz, 2H), 8.08 (d, J = 7.5 Hz, 2H), 7.86 (t, J = 7.5 Hz, 2H), 7.18 (t, J = 6.5 Hz, 2H), 7.03 (s, 2H), 6.93 (d, J = 5.5 Hz, 2H), 4.93 (d, J = 17 Hz, 2H), 4.42 (d, J = 17 Hz, 2H); ^{19}F NMR (470 MHz, methanol-d_4, 298 K) δ −62.12 (s, 6F, CF_3). Anal. Calcd for $C_{30}H_{22}Cl_2F_6N_8Ru\cdot CH_3OH\cdot {}^1/_2CH_2Cl_2$: C, 44.25; H, 3.18; N, 13.11. Found: C, 44.26; H, 3.44; N, 13.35.

Preparation of [Ru(fpbpym)(fpbpyk)] (2). A mixture of $[Ru(DMSO)_4Cl_2]$ (77 mg, 0.159 mmol), fpbpymH (102 mg, 0.335 mmol), and Na_2CO_3 (36 mg, 0.340 mmol) in ethanol (25 mL) was refluxed for 12 h under a nitrogen atmosphere. After the mixture was cooled to room temperature, the solvent was evaporated; the residue was then subjected to silica gel column chromatography, and the product was eluted with a 2:1 mixture of CH_2Cl_2 and acetonitrile. Complex **2** was further purified by recrystallization from a 1:3 mixture of acetone and hexane at room temperature. Yield: 40 mg, 0.0554 mmol, 35%. Single crystals were obtained by the slow diffusion of an n-hexane solvent into the acetone solution of **2**.

Spectral data for 2: MS (FAB, ^{101}Ru) m/z 723 ($M^+ + 1$); IR (KBr) ν(CO) 1628 cm^{-1}; ^1H NMR (500 MHz, CD_3CN, 298 K) δ 8.84 (d, J = 8.5 Hz, 1H), 8.54 (d, J = 8.5 Hz, 1H), 8.39 (d, J = 7.5 Hz, 1H), 8.25−8.17 (m, 3H), 8.12 (t, J = 8.0 Hz, 1H), 7.79 (d, J = 8.5 Hz, 1H), 7.65−7.61 (m, 3H), 7.37 (d, J = 5.5 Hz, 1H), 7.14 (s, 1H), 7.00 (t, J = 6.5 Hz, 1H), 6.96 (t, J = 6.5 Hz, 1H), 6.10 (s, 1H), 4.79 (d, J = 17 Hz, 1H), 4.54 (d, J = 17 Hz, 1H); ^{19}F NMR (470 MHz, CD_3CN, 298 K) δ −60.03 (s, 3F, CF_3), −61.31 (s, 3F, CF_3). Anal. Calcd for $C_{30}H_{18}F_6N_8ORu$: C, 49.94; H, 2.51; N, 15.53. Found: C, 49.75; H, 2.89; N, 15.30.

Preparation of $[Ru(fpbpyk)_2]$ (3). Method A. A mixture of $[Ru(DMSO)_4Cl_2]$ (83 mg, 0.171 mmol), fpbpymH (112 mg, 0.368 mmol), and Na_2CO_3 (57 mg, 0.538 mmol) in 25 mL of diethylene glycol monoethyl ether (DGME) was heated at 170 °C for 24 h under a nitrogen atmosphere. After the mixture was cooled to room temperature, the solvent was removed under vacuum, and the residue was subjected to alumina oxide column chromatography, eluting with a 9:1 mixture of CH_2Cl_2 and acetonitrile. Complex **3** was further purified by recrystallization from a 1:5 mixture of acetone and diethyl ether at room temperature. Yield: 45 mg, 0.0612 mmol, 36%. Single crystals were obtained by the slow diffusion of n-hexane into an acetone solution of **3**.

Method B. A mixture of **2** (10 mg, 0.0138 mmol) and Na_2CO_3 (15 mg, 0.141 mmol) in ethanol (25 mL) was refluxed for 12 h under an oxygen atmosphere. Application of similar workup procedures gave isolation of 8.5 mg of **3** (0.0115 mmol, 83%).

Method C. A mixture of $[Ru(DMSO)_4Cl_2]$ (36 mg, 0.0743 mmol), fpbpymH (49 mg, 0.161 mmol), and Na_2CO_3 (31 mg, 0.292 mmol) in 10 mL of DGME was heated at 170 °C for 12 h under an oxygen atmosphere. Application of similar workup procedures gave isolation of 40 mg of **3** (0.054 mmol, 73%).

(15) Rau, S.; Schwalbe, M.; Losse, S.; Görls, H.; McAlister, C.; MacDonnell, F. M.; Vos, J. G. *Eur. J. Inorg. Chem.* **2008**, 1031.

(16) (a) Abrahamsson, M.; Lundqvist, M. J.; Wolpher, H.; Johansson, O.; Eriksson, L.; Bergquist, J.; Rasmussen, T.; Becker, H.-C.; Hammarström, L.; Norrby, P.-O.; Åkermark, B.; Persson, P. *Inorg. Chem.* **2008**, *47*, 3540. (b) Schramm, F.; Meded, V.; Fliegl, H.; Fink, K.; Fuhr, O.; Qu, Z.; Klopper, W.; Finn, S.; Keyes, T. E.; Ruben, M. *Inorg. Chem.* **2009**, *48*, 5677.

(17) Garber, T.; Van Wallendael, S.; Rillema, D. P.; Kirk, M.; Hatfield, W. E.; Welch, J. H.; Singh, P. *Inorg. Chem.* **1990**, *29*, 2863.

(18) (a) Wolfe, J. F.; Murray, T. P. *J. Org. Chem.* **1971**, *36*, 354. (b) Pasquinet, E.; Rocca, P.; Godard, A.; Marsais, F.; Quéguiner, G. *J. Chem. Soc., Perkin Trans. 1* **1998**, 3807. (c) Savage, S. A.; Smith, A. P.; Fraser, C. L. *J. Org. Chem.* **1998**, *63*, 10048.

(19) Constable, E. C.; Heirtzler, F.; Neuburger, M.; Zehnder, M. J. *J. Am. Chem. Soc.* **1997**, *119*, 5606.

Table 1. Crystal Data and Structural Refinement Parameters for Complexes **1**−**4**

	1·2CH_2Cl_2·H_2O·$^3/_4CH_3OH$	**2**·C_6H_{14}	**3**	**4**·2C_3H_6O
empirical formula	$C_{32.75}H_{31}Cl_6F_6N_8O_{1.75}Ru$	$C_{33}H_{25}F_6N_8ORu$	$C_{30}H_{16}F_6N_8O_2Ru$	$C_{36}H_{28}F_6N_8O_4Os$
fw	992.43	764.68	735.58	940.86
T (K)	150(2)	293(2)	150(2)	150(2)
cryst syst	monoclinic	monoclinic	monoclinic	monoclinic
space group	$P2_1/c$	$C2/c$	$P2_1/c$	$P2_1/n$
a (Å)	16.6428(2)	21.4805(3)	9.7564(4)	14.3862(2)
b (Å)	27.0851(4)	16.2765(3)	12.2193(5)	16.6975(2)
c (Å)	19.3011(2)	17.7118(2)	23.9532(10)	15.0748(2)
β (deg)	104.4235(7)	93.7405(10)	100.349(1)	104.6891(7)
V (Å^3), Z	8426.16(18), 8	6179.34(16), 8	2809.2(2), 4	3502.82(8), 4
ρ_{calcd} (g cm^{-3})	1.565	1.644	1.739	1.784
abs coeff (mm^{-1})	0.819	0.587	0.644	3.726
F(000)	3980	3080	1464	1848
cryst size (mm^3)	0.35 × 0.16 × 0.13	0.28 × 0.14 × 0.08	0.20 × 0.15 × 0.15	0.30 × 0.25 × 0.17
reflns collcd	36 024	18 749	21 264	22 328
indep reflns [R(int)]	14 841 [0.0372]	7069 [0.0498]	6448 [0.0461]	8031 [0.0496]
max, min transm	0.913, 0.781	0.951, 0.870	0.9095, 0.8819	0.553, 0.253
data/restraints/param	14 841/15/998	7069/2/428	6448/0/424	8031/6/487
GOF on F^2	1.048	1.029	1.114	1.017
final R indices [$I > 2\sigma(I)$]	R1 = 0.0959, wR2 = 0.2875	R1 = 0.0428, wR2 = 0.1051	R1 = 0.0524, wR2 = 0.105	R1 = 0.0400, wR2 = 0.1066
R indices (all data)	R1 = 0.1338, wR2 = 0.3197	R1 = 0.0987, wR2 = 0.1224	R1 = 0.0688, wR2 = 0.1127	R1 = 0.0505, wR2 = 0.1137
largest diff peak and hole (e Å^{-3})	2.379 and −1.788	0.734 and −0.585	1.077 and −0.619	2.043 and −2.024

Spectral data for 3: MS (FAB, ^{101}Ru) m/z 736 (M^+); IR (KBr) ν(CO) 1630 cm^{-1}; ^{1}H NMR (500 MHz, CD_3CN, 298 K) δ 8.89 (dd, J = 8.25 and 1.25 Hz, 2H), 8.62 (dd, J = 8.25 and 1.25 Hz, 2H), 8.31 (t, J = 8.0 Hz, 4H), 7.70 (t, J = 7.4 Hz, 2H), 7.64 (d, J = 6.0 Hz, 2H), 7.08 (s, 2H), 7.06 (t, J = 6.5 Hz, 2H); ^{19}F NMR (470 MHz, CD_3CN, 298 K) δ −61.45 (s, 6F, CF_3). Anal. Calcd for $C_{30}H_{16}F_6N_8O_2Ru$: C, 48.99; H, 2.19; N, 15.23. Found: C, 49.24; H, 2.46; N, 14.94.

Preparation of ^{18}O-Enriched 3. To a nitrogen-filled Schlenk flask was added [Ru(DMSO)$_4$Cl$_2$] (50 mg, 0.103 mmol), fpbpymH (68 mg, 0.223 mmol), Na_2CO_3 (69 mg, 0.651 mmol), and degassed DGME (10 mL). The flask was evacuated, and $^{18}O_2$ was admitted into the flask until the pressure of the $^{18}O_2$ gas reached 1 atm. The above mixture was heated at 150 °C for 24 h. After the mixture was cooled to room temperature, the solvent was removed under vacuum, and the residue was subjected to alumina oxide column chromatography, eluting with a 9:1 mixture of CH_2Cl_2 and acetonitrile. Recrystallization from a 1:5 mixture of acetone and diethyl ether gave 71 mg of **3** (0.096 mmol, 93%).

Preparation of [Os(fpbpyk)$_2$] (4). A mixture of $OsCl_3 \cdot 3H_2O$ (49 mg, 0.140 mmol) and fpbpymH (108 mg, 0.355 mmol) in 20 mL of DGME was heated at 170 °C for 24 h. After the mixture was cooled to room temperature, the solvent was removed under vacuum, and the residue was subjected to silica gel column chromatography, eluting with a 10:1 mixture of CH_2Cl_2 and acetonitrile. The product was further recrystallized from a 1:6 mixture of acetone and diethyl ether at room temperature. Yield: 37 mg, 0.045 mmol, 32%. Single crystals suitable for X-ray diffraction study were obtained by the slow diffusion of n-hexane into an acetone solution of **4**.

Spectral data for 4: MS (FAB, ^{192}Os) m/z 826 (M^+); IR (KBr) ν(CO) 1626 cm^{-1}; ^{1}H NMR (500 MHz, CD_3CN, 298 K) δ 8.84 (d, J = 8.5 Hz, 2H), 8.55 (d, J = 7.5 Hz, 2H), 8.23 (d, J = 8.0 Hz, 2H), 7.86 (t, J = 8.0 Hz, 2H), 7.55 (d, J = 5.5 Hz, 2H), 7.41 (t, J = 7.75 Hz, 2H), 6.97 (s, 2H), 6.93 (t, J = 6.25 Hz, 2H); ^{19}F NMR (470 MHz, CD_3CN, 298 K) δ −61.56 (s, 6F, CF_3). Anal. Calcd for $C_{30}H_{16}F_6N_8O_2Os$: C, 43.69; H, 1.96; N, 13.59. Found: C, 43.44; H, 2.26; N, 13.33.

X-ray Diffraction Studies. Single-crystal X-ray diffraction data of **1**−**4** were measured on a Bruker SMART Apex CCD diffractometer using Mo Kα radiation (λ = 0.710 73 Å). The data collection was executed using the *SMART* program. Cell refinement and data reduction were performed with the *SAINT* program. The structure was determined using the *SHELXTL*/*PC* program and refined using full-matrix least squares. The crystals of **1** are of relatively poor quality because of the incorporation of three different kinds of solvates in the crystal lattices, namely, CH_2Cl_2, water, and methanol; thus, its bond distances and angles showed much larger standard deviations and had to be handled with caution. The crystallographic refinement parameters of complexes **1**−**4** are summarized in Table 1.

Spectral Measurement. Steady-state absorption was recorded with a Hitachi (U-3310) spectrophotometer. For measurement of the NIR emission, a continuous-wave Ar-ion laser (514 nm, Coherent Innova 90) was used as the excitation source and was modulated at approximately 140 Hz by a mechanical chopper. The NIR emission was then recorded at a direction perpendicular to the pump beam and sent through a lock-in amplifier (Stanford Research System SR830) before being detected by an NIR-sensitive photomultiplier tube (Hamamatzu R5509-72) operated at −80 °C.

Electrochemical Measurement. Cyclic voltammetry was carried out in a three-compartment cell using a glassy carbon disk working electrode, a platinum counter electrode, and a Ag/Ag$^+$ (CH Instruments, 10 mM $AgNO_3$ in MeCN) reference electrode. All experiments were performed in dry acetonitrile with 0.1 M tertrabutylammonium hexafluorophosphate as the supporting electrolyte. Potentials are quoted versus the ferrocene/ferrocenium couple (Fc/Fc$^+$ = 0.0 V).

Computational Methodology. Density functional theory (DFT) calculations on the electronic singlet and triplet states of complexes **1**−**4** were carried out using a hybrid Hartree−Fock/density functional model (PBE1PBE) based on the Perdew−Burke−Erzenrhof (PBE) functional.[20] Restricted and unrestricted formalisms were adopted in the singlet and triplet geometry optimization calculations, respectively. A double-ζ quality basis set consisting of Hay and Wadt's effective core potentials (LANL2DZ) was employed for the Ru and Os atoms and a 6-31G* basis set for the H, C, N, O and F atoms, while a relativistic effective core potential was applied to the inner core

(20) (a) Perdew, J. P.; Burke, K.; Ernzerhof, M. *Phys. Rev. Lett.* **1996**, *77*, 3865. (b) Perdew, J. P.; Burke, K.; Ernzerhof, M. *Phys. Rev. Lett.* **1997**, *78*, 1396. (c) Adamo, C.; Barone, V. *J. Chem. Phys.* **1999**, *110*, 6158.

electrons of those heavy transition metals.[21] Time-dependent DFT (TDDFT) calculations for the $S_0 \rightarrow S_n$ and $S_0 \rightarrow T_n$ transitions using the PBE1PBE functional were then performed based on the optimized geometries at ground state to probe the emissive properties.[22] Oscillator strengths were deduced from the dipole transition matrix elements (for singlet states only). All calculations were carried out using *Gaussian 03*.[23]

Electronic configurations of ^{3}MLCT and ^{3}MC dd states were calculated following the literature methodology.[16,24] The ^{3}MLCT state geometry was obtained by geometry optimization along the triplet-state potential energy surface (PES) using the X-ray crystal structure as the initial geometry. As for the ^{3}MC dd state, because the electron densities are mainly distributed on the central metal atom, the metal−chelate bonding interaction can be neglected for simplicity. We then performed geometry optimization of the ^{3}MC dd state following the methodology illustrated in Persson's work.[16] The method starts with a distorted geometry, for which the metal−ligand bonds are largely elongated, so that its associated energy is expected to be far away from the global minimum along the PES. The resulting ^{3}MC dd structure was then confirmed by the net spin values located on the transition metal from the Mulliken population analysis. The frontier orbitals of the ^{3}MC dd states of complexes **1**−**4** are depicted in the Supporting Information (see Figures S1−S4).

The compositions of the molecular orbitals in terms of the constituent chemical fragments were calculated using the *AOMix* program.[25] For characterization of the HOMO$-x$ → LUMO$+y$ transitions as partial CT transitions, the following definition of the CT character was used:

$$\mathrm{CT(M)} = \%\mathrm{(M)HOMO}-x - \%\mathrm{(M)LUMO}+y$$

where %(M)HOMO$-x$ and %(M)LUMO$+y$ are electronic densities on the metal in HOMO$-x$ and LUMO$+y$. If the excited state, e.g., S_1 or T_1, is formed by more than one single-electron excitation, then the metal CT character of this excited state is expressed as a sum of the CT characters of each participating excitation, $i \rightarrow j$:

$$\mathrm{CT}_I\mathrm{(M)} = \sum_{i,a} [C_I(i \rightarrow j)]^2 [\%\,(\mathrm{M})_i - \%\,(\mathrm{M})_j]$$

where $C_I(i \rightarrow j)$ are the appropriate coefficients of the Ith eigenvector of the CI matrix.

3. Results and Discussion

3.1. Synthesis and Characterization. Synthesis of the homoleptic Ru^{II} complex **1** was performed using $[Ru(DMSO)_4Cl_2]$ and 2 equiv of fpbpymH in refluxing ethanol. This complex is soluble in protic solvents such as methanol. The ^{1}H NMR spectrum in CD_3OD exhibits two methylene doublets at δ 4.93 and 4.42 with J_{HH} = 17 Hz, consistent with their diastereotopic nature, together with multiple aromatic proton signals in the region δ 8.66−6.92. However, a unique NH signal was not detected, which is apparently because of its higher acidity and, hence, a faster and reversible proton dissociation upon dissolution in polar solvents. A similar phenomenon has been documented in Pt^{II} complexes possessing the related azolate chelates.[26] Structural characterization of **1** further confirms the capability of fpbpymH to act as a neutral chelate, despite of having such an acidic N−H group.[27]

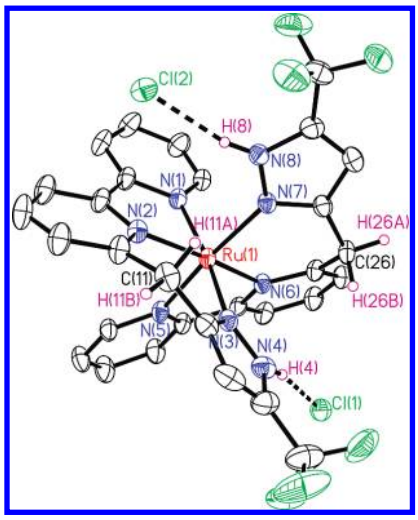

Figure 1. ORTEP diagram of **1** with thermal ellipsoids shown at 25% property level. Selective distances (Å): Ru(1)−N(1) = 2.034(8), Ru(1)−N(2) = 2.049(7), Ru(1)−N(3) = 2.061(8), Ru(1)−N(5) = 2.046(7), Ru(1)−N(6) = 2.059(7), Ru(1)−N(7) = 2.061(7), Cl(1)···H(4) = 2.190, Cl(2)···H(8) = 2.202, N(8)···H(11A) = 3.083, N(4)···H(26B) = 2.970. Bond angles (deg): N(1)−Ru(1)−N(3) = 170.7(3), N(5)−Ru(1)−N(7) = 170.3(3), N(2)−Ru(1)−N(6) = 168.1(3).

The single crystals of **1** were obtained by cooling of a supersaturated solution prepared from a 1:20 mixture of methanol and CH_2Cl_2 at room temperature. As shown in Figure 1, the structure of **1** shows a much optimized octahedral geometry compared to its parent complex $[Ru(tpy)_2]^{2+}$, for which the transoidal N−Ru−N angles are measured to be 170.7, 170.3, and 168.1° for **1** and 158, 158, and 178° for the parent $[Ru(tpy)_2]^{2+}$ complex.[28]

Moreover, both fpbpymH chelates appear as neutral ligands. In addition, these N−H protons are linked to two noncoordinated chlorides with distances Cl(1)···H(4) = 2.190 Å and Cl(2)···H(8) = 2.202 Å, showing obvious hydrogen-bonding interaction. The $Ru-N_{bpy}$ bond distances span from 2.034 to 2.059 Å, which are comparable to the average distance for Ru−N vectors in $[Ru(bpy)_3]^{2+}$ (∼2.056 Å)[29] but are longer than the middle Ru−N distances (1.974 and 1.981 Å) of $[Ru(tpy)_2]^{2+}$, showing relief of the internal strain energy. The averaged $Ru-N_{pyrazolate}$ distance is ca. 2.061 Å, which is also akin to

(21) (a) Hay, P. J.; Wadt, W. R. *J. Chem. Phys.* **1985**, *82*, 270. (b) Wadt, W. R.; Hay, P. J. *J. Chem. Phys.* **1985**, *82*, 284. (c) Hay, P. J.; Wadt, W. R. *J. Chem. Phys.* **1985**, *82*, 299.

(22) (a) Jamorski, C.; Casida, M. E.; Salahub, D. R. *J. Chem. Phys.* **1996**, *104*, 5134. (b) Petersilka, M.; Grossmann, U. J.; Gross, E. K. U. *Phys. Rev. Lett.* **1996**, *76*, 1212. (c) Bauernschmitt, R.; Ahlrichs, R.; Hennrich, F. H.; Kappes, M. M. *J. Am. Chem. Soc.* **1998**, *120*, 5052. (d) Casida, M. E. *J. Chem. Phys.* **1998**, *108*, 4439. (e) Stratmann, R. E.; Scuseria, G. E.; Frisch, M. J. *J. Chem. Phys.* **1998**, *109*, 8218.

(23) *Gaussian 03*, revision C.02; Gaussian, Inc.: Wallingford, CT, **2004**.

(24) Bark, T.; Thummel, R. P. *Inorg. Chem.* **2005**, *44*, 8733.

(25) (a) Gorelsky, S. I. *AOMix: Program for Molecular Orbital Analysis*; University of Ottawa: Ottawa, Ontario, Canada, 2007; http://www.sg-chem.net/. (b) Gorelsky, S. I.; Lever, A. B. P. *J. Organomet. Chem.* **2001**, *635*, 187.

(26) (a) Chang, S.-Y.; Chen, J.-L.; Chi, Y.; Cheng, Y.-M.; Lee, G.-H.; Jiang, C.-M.; Chou, P.-T. *Inorg. Chem.* **2007**, *46*, 11202. (b) Chang, S.-Y.; Kavitha, J.; Hung, J.-Y.; Chi, Y.; Cheng, Y.-M.; Li, E. Y.; Chou, P.-T.; Lee, G.-H.; Carty, A. J. *Inorg. Chem.* **2007**, *46*, 7064.

(27) (a) Vos, J. G.; Kelly, J. M. *Dalton Trans.* **2006**, 4869. (b) Browne, W. R.; O'Boyle, N. M.; McGarvey, J. J.; Vos, J. G. *Chem. Soc. Rev.* **2005**, *34*, 641. (c) Koo, C. K.; Lam, B.; Leung, S. K.; Lam, M. H. W.; Wong, W. Y. *J. Am. Chem. Soc.* **2006**, *128*, 16434.

(28) Lashgari, K.; Kritikos, M.; Norrestam, R.; Norrby, T. *Acta Crystallogr., Sect. C* **1999**, *C55*, 64.

(29) Rillema, D. P.; Jones, D. S.; Woods, C.; Levy, H. A. *Inorg. Chem.* **1992**, *31*, 2935.

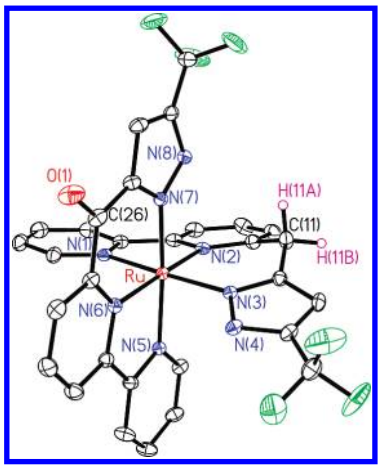

Figure 2. ORTEP diagram of **2** with thermal ellipsoids shown at 25% property level. Selective distances (Å): Ru−N(1) = 2.051(3), Ru−N(2) = 2.051(3), Ru−N(3) = 2.039(3), Ru−N(5) = 2.042(3), Ru−N(6) = 2.039(3), Ru−N(7) = 2.036(3), C(26)−O(1) = 1.224(4), N(8)···H(11A) = 2.817. Bond angles (deg): N(1)−Ru−N(3) = 172.2(1), N(5)−Ru−N(7) = 173.3(1), N(2)−Ru−N(6) = 174.2(1).

those (2.063 and 2.065 Å) observed in neutral Ru^{II} complex $[Ru(fpbpy)_2]$.[12a] Finally, one methylene proton of each fpbpymH chelate displays a shortened nonbonding contact to one pyrazolate N atom of the second fpbpymH chelate [N(8)···H(11A) = 3.083 and N(4)···H(26B) = 2.970 Å]. This intramolecular C−H···N bonding interaction is expected to increase its reactivity toward other reagents such as dioxygen present in the reaction media.

We then made attempts to conduct a reaction of **1** with Na_2CO_3 for generation of the hypothetical neutral complex $[Ru(fpbpym)_2]$. Another alternative involves heating of the metal reagent $[Ru(DMSO)_4Cl_2]$ with 2 equiv of fpbpymH in basified ethanol. Both reactions, unfortunately, failed to produce the designated $[Ru(fpbpym)_2]$ but instead afforded a purple product in ∼35% yield, which is denoted as **2**. The ^{1}H NMR analysis of **2** showed two doublets, which integrate for a total of two protons at δ 4.79 and 4.54 with J_{HH} = 17 Hz. These spectral data unambiguously indicate one methylene-to-carbonyl group conversion, as revealed by the simultaneous appearance of a ν_{CO} stretching band at 1628 cm^{-1} in its IR spectrum. Furthermore, the ^{1}H NMR spectra of **2** exhibited a total of 16 aromatic resonances in the region δ 8.84−6.10, expected for two nonequivalent bpy and two pyrazolate fragments.

As indicated in Figure 2, the structure of **2** consists of a less distorted coordination geometry versus that observed for **1**, showing bond angles of N(1)−Ru−N(3) = 172.2(1)°, N(5)−Ru−N(7) = 173.3(1)°, and N(2)−Ru−N(6) = 174.2(1)° and the absence of counteranions. For both terdentate chelates, Ru−N distances involving pyrazolates (2.036−2.039 Å) turned relatively shorter than those of the neutral bipyridine units (2.039−2.051 Å); the results can be rationalized by the increased Coulomb interaction between the cationic Ru^{II} metal center and anionic pyrazolates.[30] On the one hand, the fpbpym chelate shows a puckered geometry due to the

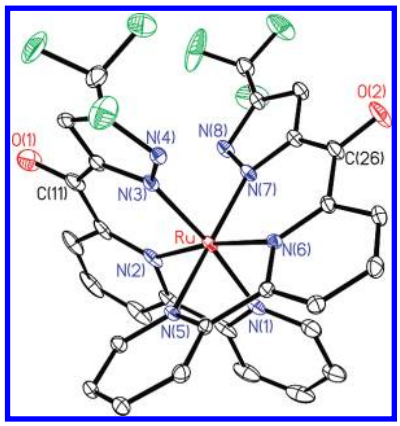

Figure 3. ORTEP diagram of **3** with thermal ellipsoids shown at 25% property level. Selective distances (Å): Ru−N(1) = 2.053(3), Ru−N(2) = 2.040(3), Ru−N(3) = 2.016(3), Ru−N(5) = 2.044(3), Ru−N(6) = 2.045(3), Ru−N(7) = 2.039(3), C(11)−O(1) = 1.226(5), C(26)−O(2) = 1.223(4). Bond angles (deg): N(1)−Ru−N(3) = 172.2(1), N(5)−Ru−N(7) = 170.9(1), N(2)−Ru−N(6) = 172.2(1).

sp^3-hybridized nature of the methylene group. On the other hand, the newly formed fpbpyk chelate reveals a planar arrangement, which is attributed to the sp^2-hybridized carbonyl group. It is also noted that the methylene group of the fpbpym chelate remains close to the uncoordinated pyrazolic N atom of the fpbpyk chelate, for which the shorter C−H···N contact of 2.817 Å implicates nonnegligible bonding interaction, similar to those observed in **1**. For a fair comparison, the sum of the van der Waals radii of N and H atoms is calculated as ∼2.8 Å.[31] Note that recent literature also reported the C−H···N hydrogen-bonding distances as ∼2.95 Å in the 3D packing of self-assembled organic materials, which provides the maximum distance for weaker C−H···N bonding.[32]

To assess the chemical stability of **2**, we conducted thermolysis in a DGME solvent at 170 °C for a period of 24 h. This harsh condition gave formation of a second charge-neutral Ru^{II} complex **3** that possesses two fpbpyk chelates. Again, the X-ray crystal structural study of **3** was examined, revealing two mutually orthogonal fpbpyk chelates. Their bonding arrangement is similar to that observed in **2** (Figure 3), except that the C−O distances span 1.223 and 1.226 Å, while both fpbpyk chelates interact with the central Ru^{II} cation with typical $Ru-N_{bpy}$ distances of 2.044−2.053 Å and $Ru-N_{pyrazolate}$ distances of 2.016 and 2.039 Å.

We further carried out the reaction of fpbpymH with the third-row congener $OsCl_3 \cdot 3H_2O$ in DGME at 170 °C, giving the doubly oxidized Os^{II} complex **4** as the sole product (Chart 3). As expected, this product showed no discernible high-field ^{1}H NMR signal attributed to the methylene protons, showing its intimate correlation to the Ru^{II} complex **3**. The single-crystal structural analysis of **4** was conducted. As shown in Figure 4, both of the skeletal arrangement and metric parameters are identical with those of **3**.

Hence, according to the chemistry established for both Ru^{II} and Os^{II} systems, the instability of **1** is believed to be

(30) (a) Tung, Y.-L.; Lee, S.-W.; Chi, Y.; Chen, L.-S.; Shu, C.-F.; Wu, F.-I.; Carty, A. J.; Chou, P.-T.; Peng, S.-M.; Lee, G.-H. *Adv. Mater.* **2005**, *17*, 1059. (b) Tung, Y.-L.; Chen, L.-S.; Chi, Y.; Chou, P.-T.; Cheng, Y.-M.; Li, E. Y.; Lee, G.-H.; Shu, C.-F.; Wu, F.-I.; Carty, A. J. *Adv. Funct. Mater.* **2006**, *16*, 1615.

(31) (a) Batsanov, S. S. *Inorg. Mater.* **2001**, *37*, 871. (b) Taylor, R.; Kennard, O. *J. Am. Chem. Soc.* **1982**, *104*, 5063.

(32) Moorthy, J. N.; Natarajan, R.; Savitha, G.; Venugopalan, P. *Cryst. Growth Des.* **2006**, *6*, 919.

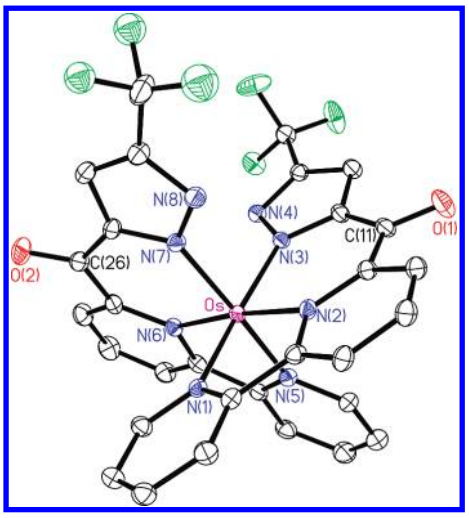

Figure 4. ORTEP diagram of **4** with thermal ellipsoids shown at 25% properties level; selective distances: Os−N(1) = 2.047(4), Os−N(2)= 2.043(4), Os−N(3) = 2.041(4), Os−N(5) = 2.044(4), Os−N(6) = 2.047(4), Os−N(7) = 2.036(4), C(11)−O(1) = 1.227(6), C(26)−O(2) = 1.224(6) Å and bond angles: N(1)−Os−N(3) = 171.4(2), N(5)−Os−N(7) = 170.9(2), N(2)−Os−N(6) = 174.4(2)°.

due to the facile oxidation capability at the fpbpymH sites. A similar increase of the chemical reactivity of N-heterocyclic chelates was also reported in the literature,[14,33] which unambiguously demonstrated that transition-metal ions can exert considerable influence on the metal-mediated or catalyzed oxygenation of alkane.

To further explore the origin of the incorporated O atom(s) in complexes **2**−**4**, a series of control and isotope-labeling experiments were carried out, including comparative reactions under regular and ^{18}O-enriched dioxygen atmospheres. Accordingly, refluxing of the ethanol solution of **2** under a dioxygen atmosphere in the presence of Na_2CO_3 afforded **3** with an improved yield to 83%. Moreover, the reaction of $[Ru(DMSO)_4Cl_2]$ with 2 equiv of fpbpymH in DGME at 170 °C under a dioxygen atmosphere also gave the doubly oxidized product **3** in 72% yield. Bearing this result in mind, we switched the oxygen atmosphere of our control reaction to the ^{18}O-enriched dioxygen and then repeated the synthesis. To our surprise, analyses of IR and FAB-MS spectral data showed no incorporation of the ^{18}O oxygen label. Therefore, the methylene-to-carbonyl conversion seems not to originate from the direct attack of the dioxygen reagent but is catalyzed by the dioxygen introduced. Unfortunately, the detailed mechanism involving the possible dioxygen participation and C−H abstraction remained unclear at the current stage.

3.2. Electrochemical Properties. The redox properties of reference complexes $[Ru(fpbpy)_2]$, $[Os(fpbpy)_2]$ (Chart 4), and **2**−**4** were next investigated in acetonitrile and with ferrocene as the internal standard, while a study of **1** was skipped because of its poor solubility in acetonitrile and greater sensitivity toward oxygen during electrochemical measurement, making the data unreliable. As depicted in Table 2, the reference complexes $[Ru(fpbpy)_2]$ and

Chart 4

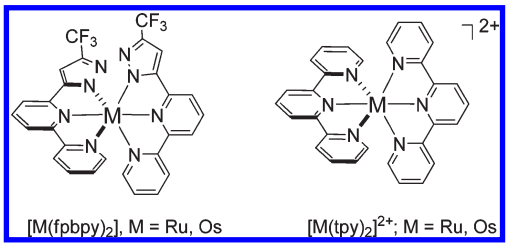

$[Os(fpbpy)_2]$ exhibit one-electron reversible oxidation peak potentials at +0.16 and −0.11 V quoted versus a Fc/Fc^+ standard and one-electron reversible reduction peak potentials at −1.97 and −1.92 V, respectively. $[Os(fpbpy)_2]$ showed a notable cathodic shift in the potential for oxidation versus that of the Ru^{II} counterpart, which is attributed to the lowered intrinsic potential of the Os^{II} metal element. In contrast, the nearly equal potential for the reduction of both complexes shows electron addition to the π^* orbital of the fpbpy chelate, which is less susceptible to the influence of the central metal atom.

On the other hand, complex **2** exhibits one-electron reversible metal-centered oxidation at 0.03 V as well as two-electron reversible waves at −1.79 and −2.19 V because of the sequential reduction occurring at fpbpyk and fpbpym chelates, respectively (see Figure S6 in the Supporting Information). In addition, both the oxidation and first reduction potentials of **2** are less and more positive compared to those of the previously discussed bis-terdentate complex $[Ru(fpbpy)_2]$, showing a reduced HOMO/LUMO energy gap. This result is in good agreement with the natural of the fpbpyk chelate, for which the carbonyl group exerts an extended π conjugation versus that of the parent fpbpy chelate. Because the carbonyl group of fpbpyk is also more electronegative, further stabilization of the metal-centered d_π orbital is expected for the fpbpyk chelate. As such, the oxidation wave for **3** (0.25 V) is more positive than that occurring for **2** (0.03 V), showing the consequence for the introduction of two (e.g., **3**) and one (e.g., **2**) fpbpyk chelates, respectively. Moreover, two less positive reduction waves at −1.71 and −1.92 V of **3** are corresponding to the one-electron reduction at each of the fpbpyk chelates. It has been reported that the anodic shifts are, in principle, exerted by localization of an electron on the carbonyl group of each terdentate chelate.[24]

Oxidation of the Os^{II} complex **4** occurs at −0.05 V, which is again more negative than that of the Ru^{II} analogue **3**, consistent with the lower potential for the third-row transition-metal elements. Likewise, the reduction waves at −1.67 and −1.93 V, which are essentially identical with those of **3**, show one-electron ligand-centered reduction occurring at each of the fpbpyk chelates. Finally, as compared to the literature data of cationic complexes $[Ru(tpy)_2]^{2+}$ and $[Os(tpy)_2]^{2+}$ (Table 2),[34] all redox potentials of **3** and **4** are found to be more negative than those recorded for the tpy analogues, a result that is attributed to the anionic charge associated with the fpbpy chelates.

(33) (a) Jitsukawa, K.; Oka, Y.; Yamaguchi, S.; Masuda, H. *Inorg. Chem.* **2004**, *43*, 8119. (b) ten Hoedt, R. W. M.; Hulsbergen, F. B.; Verschoor, G. C.; Reedijk, J. *Inorg. Chem.* **1982**, *21*, 2369. (c) Lee, D.-H.; Murthy, N. N.; Karlin, K. D. *Inorg. Chem.* **1996**, *35*, 804.

(34) Encinas, S.; Flamigni, L.; Barigelletti, F.; Constable, E. C.; Housecroft, C. E.; Schofield, E. R.; Figgemeier, E.; Fenske, D.; Neuburger, M.; Vos, J. G.; Zehnder, M. *Chem.—Eur. J.* **2002**, *8*, 137.

Table 2. Photophysical and Electrochemical Data for Ru^{II} and Os^{II} Complexes **1**−**4** and Relevant Reference Samples in an Acetonitrile Solution

compound	abs λ_{max}/nm ($\varepsilon \times 10^{-3}$/[$M^{-1}cm^{-1}$])	em λ_{max}/nm[a]	$E_{1/2}^{ox}$	Φ_p[e]	$E_{1/2}^{red}$/V [ΔE_p/mV][b]
$[Ru(fpbpy)_2]$	400 (9.1), 472 (6.4), 511 (7.7), 635 (1.4)		0.16 [53]		−1.97 [53]
$[Os(fpbpy)_2]$	465 (9.9), 650 (2.8), 715 (2.9)	(935)[d]	−0.11 [68]		−1.92 [73]
1	246 (1.43), 294 (3.46), 467 (0.49)	666 (612)		0.082	
2	255 (2.20), 299 (3.73), 518 (0.85)	810 (750)	0.03 [52]	0.012	−1.79 [52], −2.19 [60]
3	271 (2.85), 310 (3.50), 507 (1.01), 629 (0.23)	795 (728)	0.25 [70]	0.020	−1.71 [60], −1.92 [59]
4	273 (2.74), 312 (3.27), 508 (0.83), 775 (0.27)	994 (955)	−0.05 [57]	0.007	−1.67 [65], −1.93 [56]
$[Ru(tpy)_2]^{2+}$	269 (4.1), 307 (5.2), 475 (1.26)	(598)	0.92	0.48[f]	−1.58, −1.82
$[Os(tpy)_2]^{2+}$	310 (7.4), 475 (1.5), 656 (0.42)	(689)	0.58		−1.63, −1.95

[a] Emissions were measured using a solid-state (powder) sample at room temperature. [b] Potentials were quoted versus the Fc/Fc^+ reference; oxidation and reduction potentials were measured in acetonitrile; ΔE_p is defined as E_{ap} (anodic peak potential) − E_{cp} (cathodic peak potential), and these data are quoted in millivolts. [c] Data were measured in an alcohol solution. [d] The numbers in parentheses were measured in the 77 K methanol glass. [e] Data were measured in the 77 K methanol glass. [f] See ref [4a].

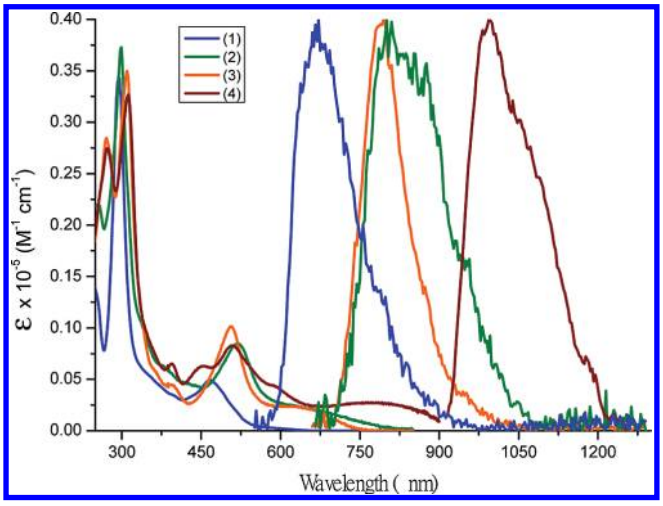

Figure 5. Absorption spectra in an acetonitrile solution and normalized solid-state (powder) emission spectra of complexes **1**−**4** recorded at room temperature.

3.3. Photophysical Properties. Pertinent photophysical data of all titled complexes **1**−**4** are also collected in Table 2, and the absorption spectra recorded in CH_3CN are depicted in Figure 5. In general, complexes **1**−**4** possess allowed absorption bands in the UV region of < 375 nm, for which ε values at the absorption maxima were measured to be $> 10^4$ M^{-1} cm^{-1} and can thus be attributed to the ligand-centered $^1\pi\pi^*$ transitions of the chelates, i.e., fpbpymH, fpbpym, and fpbpyk. Next, the lower-lying absorption band with peak wavelengths at 400−600 nm can be reasonably assigned to a spin-allowed MLCT transition in the singlet manifold. The carbonyl functionality in the fpbpyk chelate, in part, elongates the π conjugation and hence decreases the MLCT gap (vide infra). Thus, complexes **2**−**4** containing the fpbpyk chelate showed the ^{1}MLCT absorption being further red-shifted from that of complex **1**. The much longer wavelength absorption band observed in **4** (cf. **1**−**3**) is consistent with the oxidation potential of Os^{II} being ∼0.3 V more negative than that of the Ru^{II} analogue **3** (see section 3.2).

As for the emission, the releasing of strained chelating bite angles for **1**−**4** is thought to have significant effects on improving the emission quantum yields. In contrast, the emission for the titled complexes **1**−**4**, i.e., the phosphorescence, is too weak to be resolved in either an aerated or a degassed solution at room temperature. This result is intriguing. Because the emission is expected to be in NIR, one may promptly mull that the emission is subject to dominant quenching via certain potential nonradiative pathways: (i) intersection with dd repulsive PES and (ii) operation of the energy gap law,[35] stating that the electronic transition with a low energy gap may be quenched by either high-frequency vibrational modes or the low-frequency, high-density vibrational overlaps. The latter path of ii may mainly be attributed to the hindered vibration of the methylene or carbonyl group associated with the fpbpym or fpbpyk ligands. However, except for **1**, pathway i is not quite possible because of the far separation between ^{3}MLCT and ^{3}MC dd states (vide infra). As for ii, the large amplitude, low-frequency vibrations, in theory, may be subsided in the rigid solid state. As a result, in the solid state, moderate emissions appear for complexes **2**−**4** at room temperature (see Figure 5). This viewpoint is also supported by the emission of **2**−**4** resolved in the 77 K MeOH glass, which showed a slight blue-shifted emission (see Figure S5 in the Supporting Information and Table 2). Moreover, the emission quantum yields span the range from 0.012 to 0.007 (cf. **2** and **4**), which are far less efficient than that for $Ru(tpy)_2^{2+}$ in 77 K methanol glass ($\Phi = 0.48$).[4a] Because moderate/weak emission was still observed, it is thus confirmed that the nonradiative decay, in certain part, is governed by the high-frequency vibrational modes, i.e., the operation of energy gap law, because of the low energy gap. For **1**, the emission yield in the 77 K methanol glass was measured to be ∼0.08. In addition to pathway ii, we demonstrate in the Computational Methodology section that the ^{3}MC dd state may also play a role in emission quenching.

The trend of the emission peak wavelength [666 nm (**1**) < 795 nm (**3**) < 810 nm (**2**) < ∼1000 nm (**4**)] among titled complexes in the solid state is in agreement with the corresponding onset of absorption spectra of **1** < **3** < **2** < **4**. To gain more insight into the photophysical properties of these NIR luminescent Ru^{II} and Os^{II} complexes, the TDDFT method is applied on the basis of the optimized ground-state structures for all four complexes to calculate the properties of the low-energy electronic transitions. Major frontier orbitals involved in the low-lying transitions are depicted in Figure 6, while the

(35) (a) Kober, E. M.; Caspar, J. V.; Lumpkin, R. S.; Meyer, T. J. *J. Phys. Chem.* **1986**, *90*, 3722. (b) Treadway, J. A.; Loeb, B.; Lopez, R.; Anderson, P. A.; Keene, F. R.; Meyer, T. J. *Inorg. Chem.* **1996**, *35*, 2242.

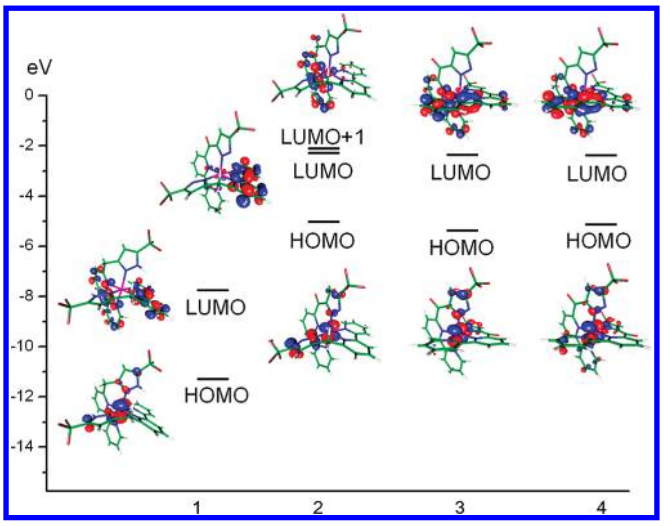

Figure 6. Frontier orbitals of complexes **1**−**4** that were involved in the $S_0 \rightarrow S_1$ and $S_0 \rightarrow T_1$ transitions.

Table 3. Calculated Energy Levels and Orbital Transition Analyses of Complexes **1**−**4**

complex	states	λ_{cal}	f	assignment	MLCT (%)
1	T_1	517.3	0	HOMO → LUMO (+92%)	59.90
	S_1	490.5	0.0054	HOMO → LUMO (+98%)	63.81
2	T_1	732.4	0	HOMO → LUMO (+90%) HOMO → LUMO+1 (+8%)	46.18
	S_1	689.6	0.0186	HOMO → LUMO (+91%)	43.10
3	T_1	665.6	0	HOMO → LUMO (+94%)	45.73
	S_1	614.8	0.0252	HOMO → LUMO (+89%)	43.30
4	T_1	807.5	0	HOMO → LUMO (+98%)	48.72
	S_1	699.1	0.0317	HOMO → LUMO (+83%)	35.33

calculated properties, such as energy gaps in terms of wavelength (λ), oscillator strengths (f), and corresponding transition assignments, are listed in Table 3. For all complexes, the calculated lower-lying transitions match well with respect to the experimental results. For example, the S_1 states of **1**−**4** are calculated to be around ~490, 690, 615, and 700 nm, the values of which are all close to the observed onsets of the absorption spectra recorded in an acetonitrile solution. The calculated S_0-T_1 gaps of **1**−**4** (**1**, 517 nm; **2**, 730 nm; **3**, 665 nm; **4**, 807 nm) are also qualitatively in agreement with the blue edge of their emission spectra recorded in the solid state (powdery samples) as well as in the 77 K methanol glass.

As listed in Table 3, the lowest singlet and triplet excited states (S_1 and T_1) for all four complexes are primarily attributed to the HOMO → LUMO transition, for which the HOMO of **1**−**4** is mainly localized at the central metal atom and, in part, the pyrazolate moiety, while the LUMO is mainly located in the bipyridyl moiety, implying that the lowest-lying transition involves MLCT mixed with an intraligand charge-transfer transition. Both HOMO and LUMO energies of **1** are apparently lower than those of other complexes due to the 2+ positive charge associated with the metal center. Figure 6 also depicts the difference of the HOMO energy between Ru^{II} (**3**) and Os^{II} (**4**) complexes under the same ligand environment. Clearly, compared to the Ru^{II} metal atom, the lower oxidation state of the Os^{II} atom leads to a higher HOMO energy for **4**, consistent with the electrochemical

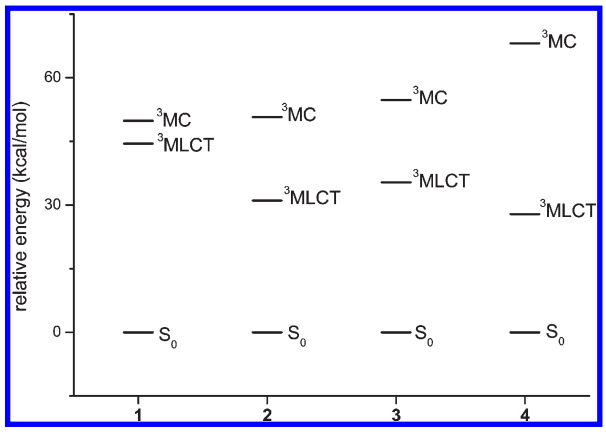

Figure 7. Energy diagram of complexes **1**−**4**. ^{3}MLCT indicates the lowest triplet electronic state obtained from unrestricted optimization, starting from X-ray crystal structures. The ^{3}MC dd state is also refined by the same method, but the initial structure is from a largely distorted geometry; see the text for a detailed description.

result of the lower oxidation potential in **4** (vide supra) and hence the smallest energy gap for the phosphorescence.

Finally, upon elongation of the chelate π conjugation, the proof of concept for tuning the relative energy gap between the ^{3}MLCT emitting and ^{3}MC dd states is elaborated for all complexes. In this approach, the higher-lying ^{3}MC dd states were calculated following methodology illustrated by Persson.[16] Details of the calculation are described in the Experimental Section. The result shown in Figure 7 clearly indicates that the replacement of fpbpymH chelates in **1** with at least one fpbpyk chelate in **2**−**4** renders better π conjugation on the coordination sphere. The net result is to decrease the energy of the π^* orbital and hence the reduction of the ^{3}MLCT energy level in **2**−**4**, whereas the ^{3}MC dd state is much less affected. This leads to an increase of the energy gap between the ^{3}MLCT and ^{3}MC dd states for **2**−**4** than that for **1**, as shown in Figure 7. In fact, because of the proximity in the energy level for **1**, the ^{3}MLCT → ^{3}MC → S_0 radiationless deactivation process, in part, may account for its extremely weak emissive nature in solution at room temperature. In contrast, this process is less thermally accessible, as evidenced by the good emission yield (~0.08; Table 2) of **1** in the 77 K matrix. Finally, despite the fact that a larger gap is observed between the ^{3}MLCT and ^{3}MC dd states for **2** and likewise **3** and **4**, emission was only slightly improved for **2**−**4** in methanol at 77 K simply because of their near-IR emission gap, which is subject to vibrational quenching.

4. Conclusions

In conclusion, a new series of bipyridyl−pyrazolate chelates and the corresponding Ru^{II} and Os^{II} complexes **1**−**4** were designed and synthesized. The exact molecular structures of **1**−**4** have been well-established by a single-crystal X-ray diffraction study. Complex **1** is readily oxygenated and converted to **2**, showing the formation of one fpbpyk chelate bearing the carbonyl group, which is produced by methylene oxidation on the terdentate fpbpymH chelate. Upon a further increase in the temperature and extension of the reaction time, the moderately stable **2** can be further oxidized to the thermodynamic product **3** with two oxygenated fpbpyk chelates. It is believed that the oxidation of the methylene

may originate from an intramolecular C−H···N interaction between one methylene proton and the pyrazolate N atom of the adjacent fpbpymH chelate, as well as the yet unexplored catalytic effect associated with both a centered metal cation and the dioxygen introduced. Thus, oxidative conversion from fpbpymH to fpbpyk chelate caused significant alterations on the inherent properties of the corresponding metal complexes. Finally, all complexes exhibit >600−1100 nm far-visible and NIR emission in the solid state at room temperature, of which the spectral features can be well rationalized by the associated electronic transition properties. Changes in the emission property, in part, are due to the incorporation of a carbonyl group that increases π conjugation and releases the internal constraint between the metal and terdentate ligand. We thus believe that the results presented here might provide new insight into the further design of flexible terdentate bipyridyl pyrazolate ligands used in the preparation of Ru^{II} and Os^{II} complexes with potentially high luminescent efficiency in the NIR region.

Acknowledgment. This work was supported by the National Science Council and Ministry of Economic Affairs of Taiwan. We are also grateful to the National Center for High-Performance Computing for computer time and facilities.

Supporting Information Available: X-ray crystallographic data files (CIF) of complexes **1**−**4**, frontier orbital distributions and net spin values from DFT calculation, emission spectra, and electrochemical spectra of the relevant complexes. This material is available free of charge via the Internet at http://pubs.acs.org.